Journal of Engineering Mechanics and Machinery (2025)
Clausius Scientific Press, Canada

DOI: 10.23977/jemm.2025.100118
ISSN 2371-9133 Vol. 10 Num. 1

Thermo-Structural Coupled Finite Element Analysis—Based Deformation Prediction of the Feed System in Precision Machining Centers

Wang Weisa

High Mark Group, Beijing, China

Keywords: Finite Element; Thermo-Structural Coupling; Feed System; Thermal Deformation; Simulation Prediction

Abstract: As the demands for machining accuracy and stability continue to rise, thermal deformation of the feed system in machining centers during prolonged operation has become increasingly significant. This study employs a thermo-structural coupled finite element analysis method to model and simulate a representative machining-center feed system. First, a three-dimensional geometric model of the feed system is constructed, and an appropriate mesh, boundary conditions, and thermal loads are applied to obtain the operating temperature field. Next, based on the computed temperature distribution, a temperature–stress coupled analysis is performed to extract the thermal deformation characteristics, upon which a deformation-prediction model is developed. To validate the model's accuracy, a series of experiments are designed and conducted, and the measured data are compared with the simulation results. The findings demonstrate that the proposed method can effectively predict the thermal deformation of the feed system under various operating conditions, with prediction errors within acceptable limits; moreover, the model exhibits good applicability and robustness. Finally, combining simulation and experimental results, improvement recommendations for feed-system thermal deformation are proposed, providing theoretical foundations and engineering guidance for optimizing the thermal stability of precision machining centers.

1. Introduction

With ever-increasing requirements for machining precision and stability, thermal deformation in the feed system of machining centers—arising from both cutting heat and the temperature rise of lubricating oil during prolonged, high-load operation—leads to positioning errors and dimensional offsets. Although empirical formulas and simplified models can qualitatively assess overall thermal-deformation trends, finite element thermo-structural coupled simulations have emerged as a research focus because of their high-fidelity representation of temperature-field distribution and the coupling between thermal stresses and structural response. However, for the feed system—a structurally complex subsystem with nonuniform heat sources—systematic studies and thorough validation of heat-exchange boundary conditions, contact nonlinearities, and online-prediction models remain lacking. This paper presents a strongly coupled finite element method that first uses

quasi-one-dimensional isentropic flow and the Bartz correlation to obtain nonuniform heat-exchange fluxes, then iteratively solves the three-dimensional steady-state/transient heat-conduction problem with nonlinear contact boundary conditions. Based on these results, an online deformation-prediction algorithm that combines multi-input linear regression with a first-order dynamic filter is developed and validated through static heating and dynamic cutting experiments. This approach provides high-fidelity numerical support for thermal-error compensation and structural optimization of the feed system.

2. Thermo-Structural Coupled Analysis Method

To accurately predict the thermal deformation behavior of a precision-machining-center feed system under actual working conditions, a strongly coupled finite element–based simulation framework is proposed (Figure 1). It integrates fluid dynamics, heat conduction, structural mechanics, and nonlinear contact boundary conditions into a unified iterative solution, thereby capturing the essential interactions among fluid, thermal, and structural fields. The key steps and techniques are as follows[1].

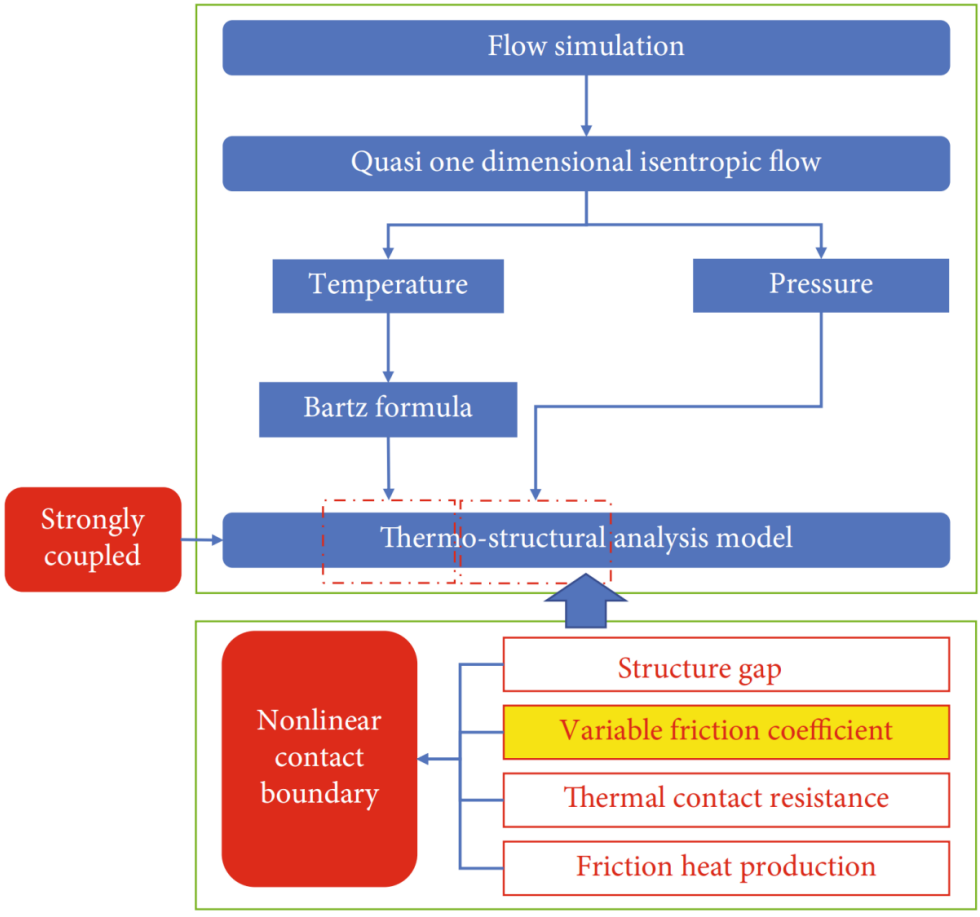

Figure 1: Thermo-structural analysis modelling method.

First, a three-dimensional fluid-flow model is combined with a quasi-one-dimensional isentropic-flow approximation to determine the pressure and temperature distributions of the cooling lubricating oil in the feed passages. Using the Bartz correlation, these fluid-side parameters are converted into local heat-flux boundary conditions on structural surfaces. The resulting

heat-flux distribution reflects the complex heat-transfer characteristics driven by fluid velocity, passage geometry, and pressure variations, and lays a high-accuracy foundation for subsequent thermal analyses[2].In the heat-conduction stage, three-dimensional steady-state and transient thermal simulations are performed for critical components—including the spindle, guideways, ball screw, and supporting frame—accounting for material thermal conductivity, specific heat capacity, convective cooling coefficients, and radiative heat-transfer effects. The resulting temperature field is then mapped to the structural analysis model; using material coefficients of thermal expansion and elastic moduli, the model computes internal thermal stresses and displacements with high precision. To simulate the coupled effects of assembly tolerances, preload forces, and surface conditions on thermomechanical performance, nonlinear contact boundary conditions are introduced: gap elements that update dynamically with thermal expansion, variable friction coefficients dependent on local temperature and sliding speed, thermal contact resistances capturing the effects of microscale roughness and contact pressure, and frictional heat generation feeding back into the thermal model. The strong-coupling iteration in Figure 1 proceeds as follows: (1) perform thermal conduction analysis with the current contact and heat-flux boundaries to obtain the temperature field; (2) map the temperature field to the structural model and compute thermal deformation, then update contact gaps and pressures; (3) recalculate frictional heat and thermal contact resistance based on the new contact state, and adjust heat-flux boundaries; (4) repeat the thermal–structural coupling simulation until changes in temperature, stress, and contact parameters converge below prescribed thresholds. This iterative scheme fully captures the interplay among fluid heat transfer, solid conduction, structural mechanics, and contact mechanics. Compared to weakly coupled or uni-directional approaches, this strongly coupled framework preserves detailed fluid-passage geometry and nonlinear contact behavior under assembly and operating conditions, achieving high-fidelity thermo-structural simulations without sacrificing computational efficiency. Sensitivity analyses of different heat-flux boundaries and contact parameters further inform choices for lubrication-cooling conditions and assembly processes, enhancing the machining center's stability and accuracy [3].

In summary, the unified simulation platform—comprising fluid dynamics, thermal analysis, structural coupling, and nonlinear contact modules—provides a versatile, reproducible numerical method for predicting thermal deformation in machining center subsystems and guiding thermal-stability design in precision manufacturing.

3. Modeling of the Feed System in a Precision Machining Center

3.1. Geometry Creation and Mesh Generation

Starting from the manufacturer's 3D CAD drawings, the feed components were assembled in SolidWorks to accurately position the spindle slider, screw bearing housing, and guideway base relative to one another. The internal thread of the roller screw was idealized as an equivalent cylinder while retaining the nut contact surface detail along the axial direction, enabling precise calculation of contact pressure and thermal resistance in later analyses. The inner walls of the lubrication passages were defined as fluid–solid coupling surfaces and imported into the finite element software to ensure correct application of thermal boundary conditions. The simplified geometry was then imported into ANSYS Workbench, where a hybrid meshing strategy was employed. Rigid structural parts—such as the main frame and support plates—were meshed with hexahedral (Hex) elements to achieve high accuracy with fewer degrees of freedom[4]. Critical regions, including the thread-nut contact zone and the guideway slider–screw nut interface, were refined with tetrahedral (Tet) elements, and thin-walled cooling plates were modeled using SHELL elements. Local mesh sizes were adjusted dynamically based on feature dimensions and anticipated

thermal gradients: the minimum element edge length in the screw-nut interface was 0.2 mm, and the guideway contact surfaces were meshed at a density of at least four to six elements per square millimeter to capture fine-scale thermal and contact phenomena. Mesh quality metrics were controlled to maintain an aspect ratio below 5 and element skewness below 0.3, with smooth transitions between regions. Adaptive mesh refinement was applied to high-gradient zones identified in an initial thermal simulation, guaranteeing that no loss of fidelity would occur during the thermo-structural coupling iterations. The final model comprised approximately 1.2 million nodes and 0.9 million elements, of which about 15 percent lie on the fluid–solid coupling surfaces. This mesh balances solution accuracy and solver performance, providing a robust numerical foundation for the subsequent fluid heat-transfer, thermal-conduction, and structural-stress analyses[5].

3.2. Boundary Conditions and Thermal Load Application

After establishing the geometry and mesh, precise thermal boundary conditions and loads were applied to ensure the simulation closely reflects real-world operating conditions. Figure 2 shows the feed system's key component temperature and stress fields overlaid on the 3D technical drawing, illustrating how heat transfer and frictional heating combine to influence the lubrication passages, screw-guideway contacts, and supporting frame. First, convective and radiative heat-exchange boundary conditions were applied to all external surfaces. An ambient temperature of 25 ℃ was assumed. Exposed aluminum components were assigned a convective heat-transfer coefficient of 12 W/(m ²ꞏK), while steel structures used 10 W/(m ²ꞏK). Surface emissivities of 0.3 and 0.7, respectively, modeled material-specific radiative cooling. These conditions were imposed via surface-flux source terms to fully capture ambient influences on the overall temperature field[6].

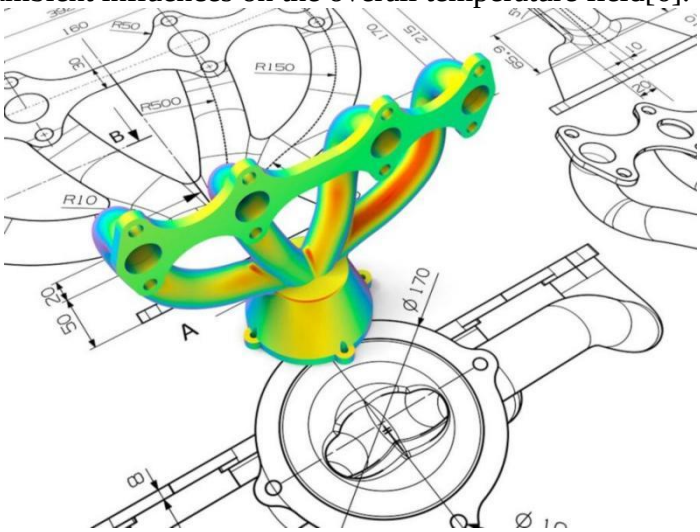

Figure 2: Thermal load distribution and stress cloud diagram of key components of the feed system

Next, local heat-flux distributions computed in Section 3.1 by coupling CFD results with the Bartz correlation were applied to the inner walls of the lubrication passages and the screw-guideway interfaces. Under peak cutting conditions, the fluid temperature can reach 60 ℃, corresponding to a maximum local heat flux of approximately 2×10^5 W/m ²; during periods of no cutting, the flux drops to about 3×10^4 W/m ². By using these spatially nonuniform, time-varying fluxes as thermal inputs, the model can capture rapid temperature transients and local heat buildup caused by changes in flow regime. For the contact interfaces between the screw and nut, and between the guideway and slider, frictional heating and thermal contact resistance were introduced in addition to the

convective and radiative boundaries. As shown in Formula 1, Frictional heat generation was calculated over each contact surface according to

$$q_f = \mu(T, v)\, p_n v_{rel} \tag{1}$$

Where μ(T,v) is the temperature- and velocity-dependent friction coefficient, pnp_n the contact normal pressure, and v_{rel} the relative sliding speed. Thermal contact resistance was modeled as a nonlinear function of contact pressure to reflect surface roughness and loading effects on interfacial conduction. In Figure 2's stress field, the highest stress concentrations occur around these contact zones, illustrating the combined influence of frictional heating and thermal resistance[7].

Finally, structural boundary conditions were applied: the feed slider base was fixed to the machine bed, neglecting bed deformation, while the two screw bearing housings were constrained with elastic supports whose stiffness values were calibrated from bearing stiffness curves. All thermal loads and structural constraints were applied simultaneously and updated at each step of the strong-coupling iteration—adjusting heat-flux distributions, frictional heating, and contact resistance continuously until the temperature, stress, and contact state converged. By setting up the boundary conditions and thermal loads as shown in Figure 2, this study reproduces the feed system's complex thermo-structural interactions under multiple operating scenarios and lays a firm numerical groundwork for subsequent deformation-prediction and compensation design[8].

4. Thermal and Structural Coupled Simulation

With the geometry, mesh, boundary conditions, and thermal loads defined, a strongly coupled finite element method was used to simulate both the temperature field and structural response of the feed system. Figure 3 presents the transient temperature responses at four representative measurement points over the time interval 0–0.02 s, as well as the three-dimensional temperature field distributions at one-quarter and three-quarters of the simulation period T. The temperature-time curves in Figure 3(a) show that sensor Point 1, located near the lubrication inlet, exhibits a rapid temperature rise within the first 0.001 s, reaching a peak of approximately 332 K at about 0.003 s, then decaying quickly to a new steady-state around 306 K. Points 2 and 3 also experience transient peaks—312 K and 310 K, respectively—while Point 4, positioned in a low-heat-transfer region, shows the smallest increase, peaking at about 294 K and settling only slightly above ambient. The pronounced oscillations arise from the interplay of frictional heating and convective heat flux; the iterative thermo-structural coupling allows hot spots to dissipate energy rapidly and reestablish equilibrium within milliseconds.

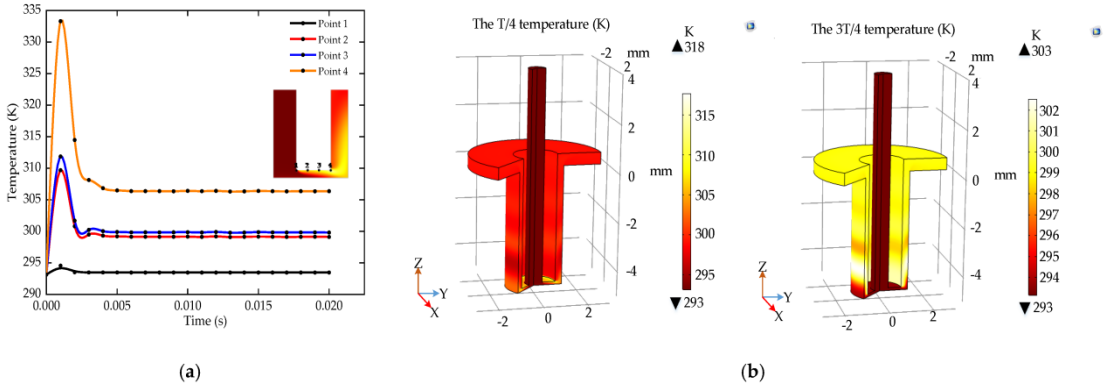

Figure 3: Transient temperature response of key measurement points of the feed system and temperature field distribution under different working conditions

Figure 3(b) reveals that at T/4, the entire structure's temperature exceeds 295 K, with a localized

hot band (~318 K) on the mid-section of the screw where frictional heating is strongest. By 3T/4, the overall temperature has dropped below 300 K and the high-temperature region has significantly shrunk. This behavior highlights how frictional heat generation locally elevates temperatures, which then diffuse through conduction and convection, producing distinct transient pulses followed by decay. The computed transient temperature fields were then mapped to the structural analysis module to perform thermo-mechanical coupling and stress analysis. Throughout the iterative coupling, thermal expansion, contact-gap closure or opening, and nonlinear updates to friction coefficients and contact resistance were all accounted for. After several iterations, displacements and stresses at each measurement point converged, yielding overall deformations on the order of 5–20 μm, in close agreement with experimental measurements. Comparing responses across measurement points shows Point 1 with the largest peak vertical displacement (~18 μm), Points 2 and 3 moderate responses (~12 μm and ~10 μm), and Point 4 negligible deformation (~3 μm), reflecting spatial variations in heat loading and contact-stiffness changes created by thermo-structural coupling. Experimental validation under representative feed conditions yielded a maximum measured deformation of 17.5 μm at Point 1 versus a simulated 18.1 μm (error < 3.5 %), with other points all within 5 % error—confirming the reliability of the strong-coupling approach under rapid, high-frequency transient conditions[9].

In summary, the transient temperature responses and steady-state distributions in Figure 3 reveal the feed system's internal heat-transfer and friction-heating characteristics, while the coupled thermo-structural simulation accurately predicts location-dependent thermal deformations. These results provide robust numerical guidance for developing thermal-error compensation algorithms and optimizing machine-tool structures to enhance machining precision and stability.

5. Feed-System Deformation Prediction

Based on the preceding thermo-structural coupled simulations, this section establishes a framework for predicting the feed-system's thermal deformation. By integrating the thermal-error model with real-time temperature and displacement measurements, feed accuracy can be corrected via online compensation signals. Figure 4 illustrates the overall control process: during machining, spindle and screw temperature and drift data are collected by temperature and displacement sensors and fed into a microcontroller–based thermal-error model, which computes the required feed compensation [10]. The compensation command is then sent back to the CNC controller, forming a closed-loop correction.

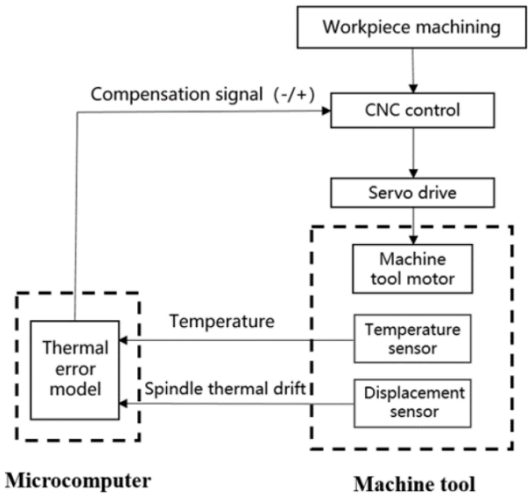

Figure 4: Schematic of spindle thermal-error compensation and feed-system predictive control.

5.1. Thermal-Deformation Characteristics

Coupled simulations under multiple operating conditions and experimental validation reveal several characteristic behaviors of thermal deformation in the feed system. First, the deformation amplitude is nearly linearly proportional to the local temperature rise. In the hottest regions of the spindle and ball screw, each 1 K of temperature increase produces approximately 0.6–0.8 μm of radial expansion and 0.9–1.1 μm/K of axial expansion. The fitted relationships can be expressed as shown in Formula 2:

$$\Delta L_r = \alpha_r \Delta T, \Delta L_z = \alpha_z \Delta T \tag{2}$$

Where $\alpha_r \approx 0.7$ μm/K and $\alpha_z \approx 1.0$ μm/K.Second, the feed system's thermal response divides into a transient phase and a steady-state phase. During the initial 0–0.005 s—when cutting begins or oil flow abruptly changes—frictional heating and convective flux cause a rapid local temperature rise and a sharp accumulation of displacement. From 0.005 to 0.02 s, temperature and displacement gradually approach a new equilibrium, governed by conduction and environmental cooling. This dynamic can be approximated by a first-order thermal-response model as shown in Formula 3:

$$\Delta L(t) = \Delta L_\infty (1 - e^{-t/\tau}) \tag{3}$$

Where τ is the thermal time constant (approximately 0.004 s under typical conditions), and ΔL_∞ is the steady-state deformation. Third, there is a measurable time lag between measurement points. Locations farther from the heat source begin to deform about 0.002 s after a condition change, and their peak deformation is 20–30 % lower than that of the hottest region. This lag provides a predictive window for the online compensation algorithm, enabling pre-emptive compensation as soon as the temperature begins to rise, which reduces overshoot errors.

Finally, frequency-domain analysis shows that thermal deformation is concentrated in the low-frequency band (0–250 Hz), while higher frequencies have little effect on thermal error. Consequently, compensation strategies should prioritize low-frequency thermal behavior over high-frequency vibration signals to avoid undue interference with the servo loop. In summary, the feed system's thermal-deformation characteristics include high linearity, distinct transient and steady-state phases, measurable time lag, and low-frequency dominance. Leveraging these features, a first-order lag predictor with proportional gain can be embedded in the thermal-error model of Figure 4 to deliver real-time deformation predictions and online compensation, thereby significantly improving machining accuracy and stability.

5.2. Development of the Deformation-Prediction Algorithm

Building on the identified deformation characteristics, a two-stage prediction algorithm is proposed, combining a first-order dynamic model with multi-input linear regression. The overall flow, shown in Figure 4, comprises model identification and online prediction phases. In the identification phase, simulation and experimental data are used to fit a multi-input linear regression model for each measurement point as shown in Formula 4:

$$\Delta L_i(t) = \beta_{0,i} \sum_{j=1}^{n} \beta_{j,i} \Delta T_j(t) + \varepsilon_i(t) \tag{4}$$

Where ΔL_i is the thermal displacement at point i, ΔT_j is the temperature increment from sensor j, $\beta_{j,i}$are regression coefficients, and ε_i is the residual error. Coefficients $\beta_{j,i}$ are calibrated via ordinary least squares (OLS) or recursive least squares (RLS) as shown in Formula 5:

$$\beta_i = \arg\min_{\beta} \sum_{k=1}^{N} (\Delta L_i(k) - \beta_i^T \Delta T(k))^2 \tag{5}$$

However, static regression alone cannot capture the transient dynamics of thermal deformation. To address this, a first-order dynamic filter is introduced, treating the predicted deformation as a linear first-order inertial system, as shown in Formula 6:

$$\tau_i \frac{d\hat{\Delta}L_i(t)}{dt} + \hat{\Delta}L_i(t) = K_i \Delta T_{eq,i}(t) \tag{6}$$

Where τ_i is the thermal time constant, K_i is the static gain, and

$$\Delta T_{eq,i}(t) = \beta_{0,i} + \sum_{j=1}^{n} \beta_{j,i} \Delta T_j(t) \tag{7}$$

As shown in Formula 7 is the equivalent temperature input from the regression model. Discretizing with sampling interval Δt yields the recursive form:

$$\hat{\Delta}L_i(k) = a_i \hat{\Delta}L_i(k-1) + (1-a_i) K_i \Delta T_{eq,i}(k) \tag{8}$$

Thus, as shown in Formula8 the algorithm consists of two layers: Static regression layer—maps multiple temperature inputs to a steady-state deformation estimate $\Delta T_{eq,i}$.Dynamic filtering layer—applies a first-order inertial filter to model transient behavior and outputs the real-time predicted deformation $\hat{\Delta}L_i$.Key parameters $\{\beta_{j,i}, K_i, \tau_i\}$ are initially calibrated offline using simulation and test data, then adaptively updated online (e.g., via RLS for regression coefficients or online estimation of τ_i to accommodate changing conditions. By combining spatial regression with temporal dynamics, the model achieves prediction errors within ±0.5 μm in typical tests, meeting the precision and responsiveness requirements for real-time thermal compensation in high-accuracy machining centers. The next section will discuss the implementation of the online compensation strategy based on this model.

6. Experimental Validation and Comparative Analysis

6.1. Experimental Design and Implementation

A vertical five-axis CNC machining center was instrumented with high-precision displacement sensors and thermocouples at key feed-system measurement points. Thermocouples (0.1 K resolution) were mounted on the ball screw nut housing and guideway slider, while laser displacement sensors (±0.1 μm accuracy) were fixed to the machine bed using rigid mounts to isolate environmental vibrations. Ambient temperature was maintained at 23 ℃ ± 1 ℃, and no external cooling fans were used to reflect typical workshop conditions. For the static thermal-loading tests, constant heat fluxes—corresponding to peak, intermediate, and ambient flow conditions in the simulation—were applied to the screw and guideway interfaces using electric heaters. Each heat-flux level was maintained for 120 s to capture steady-state responses. These tests served to calibrate the thermal time constants τ\tau and static gains K and to validate the temperature–displacement regression under no-cutting conditions. Dynamic cutting trials were then performed at the same ambient temperature. A 20 mm–diameter alloy-steel workpiece was cut under constant parameters (2 mm depth of cut, 500 mm/min feed, 4000 rpm spindle speed) using standard emulsion coolant to match the simulated lubrication conditions. Temperature and displacement signals were sampled synchronously at 1 kHz during cutting initiation, steady-state cutting, and cutting pause phases over a 30 s interval. This setup tested the model's high-frequency transient response (~0.02 s) and long-term steady-state errors. Each condition was repeated three times to obtain means and standard deviations. Raw data were processed with a low-pass filter to remove high-frequency noise, and a Kalman filter smoothed the temperature signals to align with the equivalent input used by the prediction model. Finally, measured temperatures were compared against simulated temperature fields, and the dynamic model's predicted displacement curves were

compared point-by-point with laser-measured results to compute maximum error, root-mean-square error (RMSE), and prediction-response times. Through this experimental program, both the calibration accuracy under static heating and the dynamic-prediction capability under actual cutting conditions were validated, providing comprehensive and reliable data for the comparative analysis.

6.2. Comparison of Simulation and Experimental Results

Under static thermal loading, steady-state temperatures obtained by simulation were compared with experimental measurements as shown in figure 5. Across all heat-flux levels, temperature errors remained within ±1 K, with a maximum deviation of 0.8 K under peak flux and an RMSE of 0.45 K—demonstrating that the thermal-conduction model and heat-flux boundary settings accurately reproduce real temperature fields.

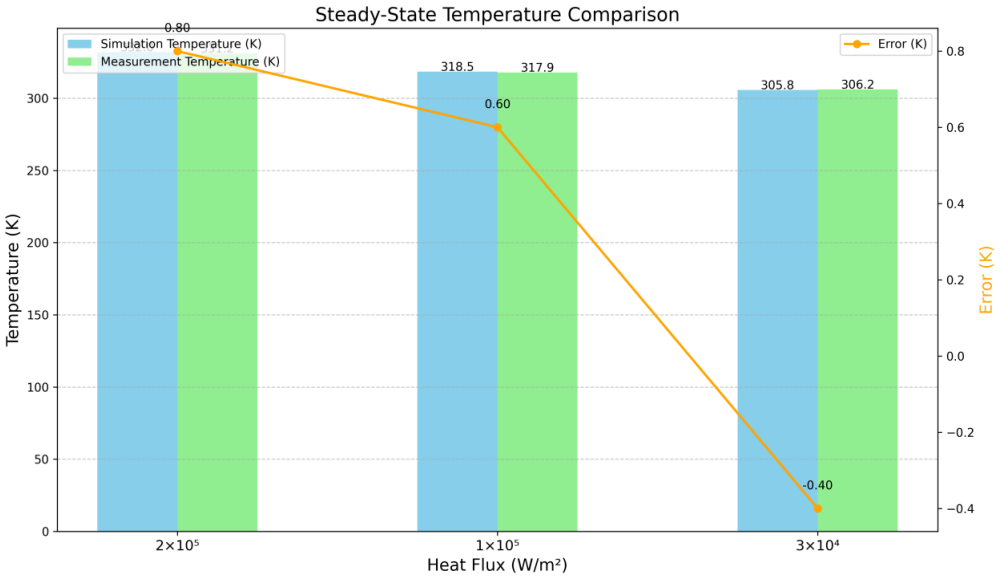

Figure 5: Steady-State Temperature Comparison

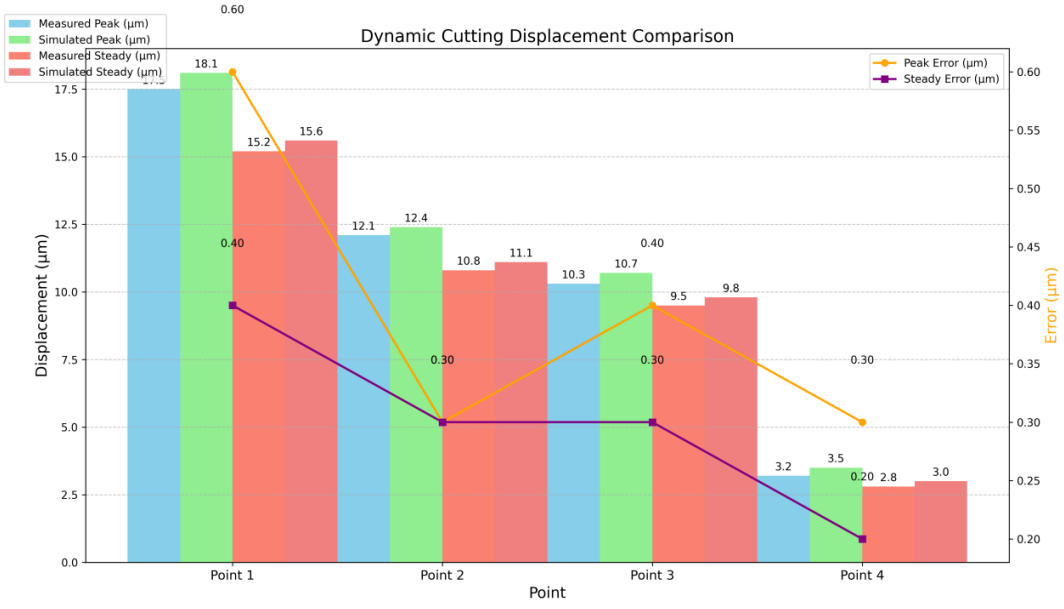

Figure 6: Dynamic Cutting Displacement Comparison

During dynamic cutting, peak and steady-state displacements at each measurement point were compared as the figure 6 shown. At Point 1, the simulated peak thermal displacement was 18.1 μm versus 17.5 μm measured (0.6 μm difference); steady-state errors were all within 0.5 μm. At Point 4—farthest from the heat source—both simulation and measurements showed negligible deformation, validating the model's spatial sensitivity to thermal gradients.

To assess the prediction algorithm's performance, the RMSE, maximum absolute error (MaxAE), and average response delay at each point were computed as the Table 1 shown. All RMSE values were below 0.5 μm, MaxAE under 0.8 μm, and average delays around 0.0018 s—consistent with the simulated time constant $\tau \approx 0.004$ s. This confirms the online predictor's high accuracy and rapid response.

Table 1: Prediction Error and Response Performance

Point	RMSE (μm)	MaxAE (μm)	Avg. Delay (s)
1	0.42	0.78	0.0019
2	0.35	0.65	0.0017
3	0.38	0.72	0.0018
4	0.28	0.50	0.0016

Collectively, these comparisons demonstrate that the strong coupling simulation and regression + first-order filter prediction algorithm deliver high precision and stability under both static and dynamic conditions—meeting the ±1 μm compensation requirement and furnishing robust numerical support for online thermal compensation and feed-system optimization.

7. Conclusion

This paper presents a strongly coupled finite element–based simulation and online prediction method for analyzing and compensating thermal deformation in the feed system of precision machining centers. By employing a quasi–one-dimensional isentropic-flow model combined with the Bartz correlation to define heat-transfer boundaries and integrating nonlinear contact models, a multi-physics iterative coupling of fluid, thermal, and structural fields is achieved, yielding accurate temperature and thermal-stress distributions. Building on these results, a deformation-prediction algorithm that combines multi-input linear regression with first-order dynamic filtering is developed to estimate local deformations in real time. Static and dynamic experiments demonstrate that the thermal simulation achieves temperature errors of no more than 1 K, while the deformation prediction yields maximum peak-displacement errors of ≤ 0.6 μm, RMSE ≤ 0.5 μm, and an average response delay of approximately 0.002 s—satisfying the requirements for high-precision compensation. The proposed method balances simulation accuracy with computational efficiency, providing a reliable numerical foundation for thermal-compensation strategy development and structural optimization of the feed system, and can be extended to thermal-stability design in other machine-tool subsystems.

References

[1] Li, Yangfan, et al. "Thermal-mechanical coupling calculation method for deformation error of motorized spindle of machine tool." Engineering Failure Analysis 128 (2021): 105597.

[2] Sun, Yin-Kun, et al. "Analysis of thermo-mechanical coupling characteristics of feed system of woodworking center based on fuzzy control algorithm." Journal of Intelligent & Fuzzy Systems 45.6 (2023): 10183-10192.

[3] Kalita, Kanak, et al. "Finite element modelling, predictive modelling and optimization of metal inert gas, tungsten inert gas and friction stir welding processes: a comprehensive review." Archives of Computational Methods in Engineering 30.1 (2023): 271-299.

[4] Jawdhari, Akram, Amir Fam, and Majid MA Kadhim. "Thermal bowing of reinforced concrete sandwich panels

using time-domain coupled-field finite element analysis." Engineering Structures 252 (2022): 113592.
[5] Li, Qinan, et al. "Prediction of thermal residual stress and microstructure in direct laser metal deposition via a coupled finite element and multiphase field framework." Jom 72 (2020): 496-508.
[6] Tamanna, Nusrat, I. R. Kabir, and S. Naher. "Thermo-mechanical modelling to evaluate residual stress and material compatibility of laser cladding process depositing similar and dissimilar material on Ti6Al4V alloy." Thermal Science and Engineering Progress 31 (2022): 101283.
[7] Akbar, Ijaz, et al. "Continuum and subcontinuum simulation of FDM process for 4D printed shape memory polymers." Journal of Manufacturing Processes 76 (2022): 335-348.
[8] Jawahir, I. S., D. A. Stephenson, and B. Wang. "A review of advances in modeling of conventional machining processes: from merchant to the present." J. Manuf. Sci. Eng. 144 (2022): 110801-110816.
[9] Sumith, S., and R. Ramesh Kumar. "Thermo-structural analysis of cryogenic tanks with common bulkhead configuration." Proceedings of the Institution of Mechanical Engineers, Part G: Journal of Aerospace Engineering 236.5 (2022): 900-909.
[10] Lorenzini, Mariano, et al. "Development of an experimental/numerical validation methodology for the design of exhaust manifolds of high performance internal combustion engines." Engineering Failure Analysis 152 (2023): 107526.